

## Microphysical Parameterization of Arctic Diamond Dust, Ice Fog, and Thin Stratus for Climate Models

ERIC GIRARD

*Department of Aerospace Engineering Sciences, University of Colorado, Boulder, Colorado*

JEAN-PIERRE BLANCHET

*Département des Sciences de la Terre et de l'Atmosphère, Université du Québec à Montréal, Montreal, Quebec, Canada*

(Manuscript received 12 July 1999, in final form 8 June 2000)

### ABSTRACT

A parameterization is described for low-level clouds that are characteristic of the Arctic during winter. This parameterization simulates the activation of aerosols, the aggregation/coalescence, and the gravitational deposition of ice crystals/water droplets and the deposition/condensation of water vapor onto ice crystals/water droplets. The microphysics scheme uses four prognostic variables to characterize clouds: ice water content, liquid water content, and the mean diameter for ice crystals and for water droplets, and includes prognostic supersaturation. The parameterization simulates stable clouds where turbulence and entrainment are weak, like ice fogs, thin stratus, and diamond dust. The parameterization is tested into the Local Climate Model (LCM), which is the single column version of the Northern Aerosol Regional Climate Model (NARCM). NARCM is a regional model with an explicit representation of the aerosol physics and with the physics package of the Canadian Climate Center General Circulation Model version two. Since most climate models do not have prognostic size-segregated aerosol representation, an alternate method is proposed to implement the microphysical parameterization into these models. The model results are compared to observations of diamond dust and ice fog at Alert (Canada) for the period 1991–94. Two aerosol scenarios are compared in the simulation: a natural background aerosol scenario and an acidic aerosol scenario. Results show that the LCM reproduces approximately the time variation of the observed weekly frequency of the total ice crystal precipitation with a correlation coefficient of 0.4. Although it overestimates diamond dust frequency and underestimates ice fog frequency, the LCM predicts quite well the total precipitation frequency (ice fog and diamond dust added). The acidic aerosol scenario is in good agreement with the observations, showing a mean frequency of total precipitation over the 4 yr of 39% compared to the observed value of 37%. The natural aerosol scenario overestimates this frequency with a value of 47%. These results were expected since recent aerosol observations have shown the predominance of sulfuric acid-coated aerosols in the Arctic during winter.

### 1. Introduction

Because of the low amount of solar energy reaching the arctic surface during winter, the boundary layer is very stable, characterized by a deep surface-based temperature inversion (Serreze et al. 1992). Under these stable conditions, observations show a frequency of up to 50% of diamond dust and ice fog at many places north of the Arctic circle from November to May. For instance, Maxwell (1982) reports a frequency varying between 20% and 50%, based on observations covering many years and for different arctic locations such as

Resolute, Mould Bay, Alert, Eureka, and Isachsen. Also, meteorological surface observations at Alert during the period 1991–1994 show a wintertime frequency of 40% of diamond dust and ice fog. According to Curry et al. (1990), these observed frequencies may be underestimated due to the difficulties of observing these phenomena during the arctic winter darkness. Satellite observations also encounter several obstacles. At visible wavelengths, suspended ice crystal reflectance is very difficult to distinguish from the snow-covered surface (Raschke 1987). Further, at infrared wavelengths, similar temperature of ice crystals and surface is a considerable obstacle (Curry et al. 1990). Consequently, actual diamond dust and ice fog frequencies may be higher than reported.

Lower-tropospheric ice crystals in the Arctic show a large range of size and concentration. Ice crystal *c* axis varies between a few microns to a few hundred microns

---

*Corresponding author address:* Eric Girard, Department of Aerospace Engineering Sciences, CB 429, University of Colorado, Boulder, CO 80309-0429.  
E-mail: girard@cires.colorado.edu

TABLE 1. Quantitative criteria used in this study to distinguish between diamond dust and ice fog.

	Diamond dust	Ice fog
Cloud particle mean diameter ( $\mu\text{m}$ )	>30	<30
Cloud particle number concentration ( $\text{L}^{-1}$ )	<4000	>1000

(Witte 1968; Ohtake et al. 1982; Trivett et al. 1988). Number concentration ranges from 1 to  $4000 \text{ L}^{-1}$ . Ice fog is distinguished from diamond dust by the large number concentration of ice crystals and their small diameter in ice fog. Quantitative criteria used to differentiate both phenomena are highly subjective. A quantitative criterion based on the liquid or ice water content has been proposed. Since the water content can be episodically very similar in both phenomena (Girard and Blanchet 2001, hereafter GB2001), criterion based on cloud water and ice content can sometimes be confusing. Two variables are used in this paper to distinguish the two phenomena: the cloud particle mean diameter and the cloud number concentration (see Table 1).

According to Curry et al. (1990), the main formation mechanism of diamond dust and ice fog in the Arctic is the advection of warm air from midlatitudes and its subsequent radiative cooling at constant pressure. This mechanism has also been recognized to be responsible for the ice crystal presence in the lower troposphere in Antarctica for a long time (Bromwich 1988). Further, Curry (1983) has shown the efficiency of this mechanism to produce observed ice crystals with numerical modeling during a transformation of a maritime air mass to an arctic air mass. However, other formation mechanisms such as (i) orographic lifting of humid air (Lax and Schwerdtfeger 1976), (ii) condensation over open leads in the sea ice (Ohtake and Holmgren 1974; Schnell et al. 1989), and (iii) humidity excess released by cities (Benson 1970) can contribute locally to the formation of diamond dust and ice fog.

Diamond dust and ice fog play an important role by controlling the radiation and moisture budget of the arctic lower troposphere (Curry et al. 1996; Beesley and Moritz 1999). By their radiative contribution, they affect sea ice thickness (Curry and Ebert 1990) and snow cover. Diamond dust dehydrates the lower troposphere and reduces the greenhouse effect (Curry 1983; Blanchet and Girard 1994, 1995). At very low temperature and high relative humidity prevailing during arctic winter, a small change in the precipitable water greatly affects the surface energy budget (Blanchet and Girard 1995; Curry et al. 1995). These particular conditions lead to 1) the decrease of the opacity of the water vapor rotational band and, 2) the shifting of the Planck function maximum toward lower frequencies. GB2001 have shown that diamond dust may contribute as much as  $60 \text{ W m}^{-2}$  to the downward infrared radiation flux at the surface in wintertime conditions. Changing the prop-

erties or the frequencies of these phenomena can have significant consequences on the arctic climate. For instance, Blanchet and Girard (1995) have shown from model simulation that a surface cooling of 5 K over 5 days is obtained due to increased precipitation efficiency during a diamond dust event. Small ice crystals of about  $30\text{-}\mu\text{m}$  diameter characteristic of ice fog lead to long-lived ice crystal clouds without any significant precipitation. Numerical modeling with a comprehensive microphysics scheme has shown that ice fog contributes substantially to the downward radiative flux at the surface (GB2001).

Intercomparison of GCM simulations of the arctic climate have shown large discrepancies between models (Walsh and Crane 1992). Surface temperature, cloud coverage, and longwave downward radiation are among the variables that show the largest uncertainty (Curry et al. 1996). For instance, Lappen (1995) conducted a detailed analysis of the Colorado State University General Circulation Model simulations of the arctic climate and comparisons with observations. She noted an overestimation of the net longwave flux at the surface caused by an underestimation of the downward longwave flux. Briegleb and Bromwich (1998) have also found a positive bias of  $10 \text{ W m}^{-2}$  when they compared National Center for Atmospheric Research Community Climate Model (NCAR CCM; Boville and Gent 1998) polar simulation to Earth Radiation Budget Experiment data for the period 1979–93. Since ice fog and clear sky ice crystal precipitation are important contributors to this flux during winter (Curry 1983; Curry et al. 1996; GB2001), they can contribute to reducing this discrepancy. Further, simulations with the Arctic Regional Climate System Model (Walsh et al. 1993) highlighted the great sensitivity of the boundary layer energy budget to the cloud microphysical parameterizations. In the context of the arctic winter, as opposed to lower latitudes where the dynamics is dominant, the lower atmosphere is very stable and cloud formation is mostly driven by radiative cooling and microphysical processes (Curry 1983). In this context, an adequate representation of phenomena such as diamond dust and ice fog is required to better simulate arctic climate.

So far, despite their radiative importance, very few efforts have been devoted to simulation of diamond dust and ice fog in climate models. Existing prognostic cloud schemes in GCMs do not allow for interaction between aerosol and cloud [see Fowler et al. (1996) for a comprehensive review]. As a result, quick changes in the supersaturation relaxation time characteristic of diamond dust events (GB2001) cannot be properly simulated by these cloud schemes. Indeed, the supersaturation relaxation time dramatically increases when the number concentration of cloud droplets and/or ice crystals decreases and when mixed phase occurs (GB2001). Furthermore, the effect of the aerosol composition and concentration on cloud formation cannot be accounted for in these simplified cloud schemes. This effect is

thought to be of less importance in convective clouds where vertical velocity is large allowing large number of aerosols to be activated. However, in stratiform clouds, in which vertical velocity is much lower, the aerosol concentration is a key factor determining the cloud particle size. Further, as shown by Bertram et al. (1996), the aerosol composition may alter the cloud phase in supercooled clouds. Therefore, there is a need to account for aerosols in the cloud formation in conditions such as those prevailing in the Arctic during winter.

Besides cloud water and ice content, the effective diameter of the cloud particles is very important in determining 1) the cloud radiative properties such as the emissivity and the albedo, 2) the ice/water ratio in the cloud, and 3) cloud lifetime. With regard to the ratio of cloud ice/cloud water, a widely used technique consists of specifying this ratio as a function of the temperature only with two threshold temperatures allowing for water phase, ice phase, and mixed phase clouds (Ghan and Easter 1992; McFarlane et al. 1992; Fowler et al. 1996). To calculate cloud optical properties, the effective radius is either specified or computed by empirical relations between cloud water content, temperature, and effective radius (e.g., Wyser 1998). Another approach consists of establishing a relationship between the aerosol number concentration and the cloud particle number concentration based on observations; however, despite having a more physical basis, this alternative has been unsuccessful in many cases (Novakov et al. 1994; Vong and Covert 1998).

Given the importance of supersaturation relaxation time and aerosol concentration and composition in the formation and evolution of the arctic low-level clouds (Curry et al. 1996; GB2001), we have developed a cloud parameterization allowing for a prognostic determination of cloud water and ice water content and the mean diameter of water droplets and ice crystals. In this paper, we present a comprehensive microphysics scheme coupled with a single column aerosol-climate model (the Local Climate Model, LCM) (Gong et al. 1997). This model simulates the aerosol time evolution explicitly and the formation of diamond dust and ice fog. In the next section, we describe the parameterization developed to represent the collision processes, the sedimentation of cloud particles, the deposition/condensation of water vapor onto preexisting ice crystals/water droplets, and the activation of aerosols. Except for the aerosol activation, these parameterizations do not require the explicit simulation of the aerosol spectrum. Since most climate models do not simulate the multicomponent aerosol size spectrum, we propose a simple alternative for the parameterization of the activation. Finally, in section 3, we compare the model results to diamond dust and ice fog observations at Alert (Canada) for the period 1991–94.

## 2. The LCM model

To develop a parameterization of the microphysics capable of simulating cold clouds in climate models,

we use observations and a comprehensive aerosol-cloud model (MAEROS2), hereafter referred to as the reference model.

### a. The reference model

A modified version of MAEROS2 (Gelbard et al. 1980) is used as the reference model. The original version of MAEROS2 has been modified to allow for ice and mixed phase clouds as well as the Kelvin effect and solution effect and extended outside the aerosol size range into the region of activated particles (GB2001). This model can simulate the time evolution of both the aerosol and cloud particle spectra. Physical processes related to aerosols, such as coagulation, sedimentation, and activation as well as processes related to cloud particles such as aggregation/coalescence, condensation/deposition, and sedimentation are explicitly simulated. Further, homogeneous and heterogeneous freezing of water droplets are accounted for, allowing representation of the phase change and also the Bergeron effect. The modified version of MAEROS2 contains 38 size bins from 0.01- to 500- $\mu\text{m}$  diameter. A complete description of this model is given in GB2001. Along with observations, the zero-dimensional version (box model) of this detailed model is used to validate the parameterization developed in this paper.

### b. General features of the LCM–NARCM model

LCM is the single column version of the Northern Aerosol Regional Climate Model (NARCM) model (Gong et al. 1997), which is a 3D regional climate model with its grid centered on the North Pole. NARCM has the same physics as the Canadian Regional Climate Model (McFarlane et al. 1992; Caya and Laprise 1999) plus the explicit aerosol scheme and a prognostic variable for each aerosol size bin and each species considered. The principal feature of the LCM model is its aerosol physics with an explicit size-segregated representation of the aerosol spectrum. Physical processes related to aerosols: coagulation, nucleation, in-cloud and below-cloud scavenging, and dry deposition are parameterized into the model (Gong et al. 1997).

#### 1) DYNAMIC TENDENCIES

The LCM is a single column model that, by definition, does not calculate dynamic tendencies explicitly. Various methods using observations and 3D model forcing to infer dynamic tendencies for single column models, such as revealed forcing, horizontal advective forcing, and relaxation forcing, are discussed by Randall et al. (1996) and Lohmann et al. (1999). However, to use these methods, one has to know the value of the advected fields at the surrounding areas. Additionally, these methods do not allow for feedbacks between the simulated physics within the column and the dynamics.

In this work, we use the residual iterative method (RIM) to infer dynamic tendencies at each time step. The RIM allows calculation of dynamic tendencies with only aerological soundings at the geographic point of interest. Note that the same method can be applied with GCM output at a particular grid point. In practice, the model is first integrated without dynamic tendencies. Output is then compared with aerological soundings at 0000 Z and 1200 Z every day, which corresponds to the time of aerological soundings. The residual, which is the difference between observations and model output, is then used as the dynamic tendencies for a second run. This technique is repeated until the change of the residual is small. The RIM converges rapidly after three or four iterations. This method has the advantage of using both the predicted value by the model and the observed value of the prognostic variable. Therefore, the model is semiprognostic, that is, the physical processes acting within the column modify the dynamics whereas the dynamics do not affect the physics. Therefore, errors in the physical parameterization are compensated by the dynamic tendencies. As a result, dynamic tendencies calculated by this method are as good as the model physics. The RIM is therefore very useful for assessing physical parameterization by ensuring that the values of prognostic fields are similar to the observations.

## 2) CLOUD PARTICLE SPECTRUM

The cloud particle spectrum is represented by the superposition of two lognormal size distributions with a standard deviation of 1.4: one for cloud droplets and the other for ice crystals. This choice of size spectrum

is based on simulations with the GB2001 reference model and observations (Witte 1968; Rogers and Yau 1989). Although observations indicate that the gamma size distribution can also be used to represent cloud spectra in models (Rogers and Yau 1989), the lognormal distribution is preferred here since it is more representative of the cloud spectra obtained with the explicit model, which has been used to develop the parameterization presented in this paper. The standard deviation of cloud particle size distribution varies according to cloud type. For instance, in diamond dust events, Witte (1968) observed standard deviation values of 1.3–1.9 discussed in GB2001. In ice or liquid stratus, the standard deviation typically ranges from 1.2 to 1.4 (Hudson and Svensson 1995; Considine and Curry 1996). In maritime liquid stratus cloud, Considine and Curry (1996) observed an increase in the standard deviation with diameter. The few available observations of diamond dust in the Arctic suggest a similar relation between the mean diameter and the standard deviation. In order to simplify the parameterization, a unique value for the standard deviation of the cloud size distribution has been chosen.

## 3) MODEL EQUATIONS

To describe cloud liquid and ice particle size distributions, four prognostic variables are used: the mean diameter of cloud droplets ( $D_w$ ), the mean diameter of ice crystals ( $D_i$ ), the cloud ice mixing ratio ( $q_i$ ), and the cloud water mixing ratio ( $q_w$ ). These parameters along with the fixed standard deviation of 1.4 describe the cloud spectrum at each time step. The time evolution of these variables can be expressed as follows:

$$\frac{\partial q_w}{\partial t} = \text{PCS} + \text{PCC} + \text{PCI} - \frac{m(D_w)}{\rho \Delta t} (\Delta N_h + \Delta N_g) + K \frac{\partial^2 q_w}{\partial z^2}, \quad (1)$$

$$\frac{\partial q_i}{\partial t} = \text{PIS} + \text{PID} + \text{PII} + \frac{m(D_w)}{\rho \Delta t} (\Delta N_h + \Delta N_g) + K \frac{\partial^2 q_i}{\partial z^2}, \quad (2)$$

$$\frac{\partial D_w}{\partial t} = \frac{1}{\Delta t} \left[ \left( \frac{-6\rho q_w}{\pi \rho_w} \right)^{1/3} \left( \frac{1}{\Delta N_h} + \frac{1}{\Delta N_g} + \frac{1}{\Delta N_{nw}} - \frac{1}{\Delta N_c} \right)^{1/3} + \left( \frac{6\Delta m_{iw}}{\pi \rho_w} \right)^{1/3} \right] + K \frac{\partial^2 D_w}{\partial z^2}, \quad (3)$$

$$\frac{\partial D_i}{\partial t} = \frac{1}{\Delta t} \left[ \left( \frac{-6\rho q_w}{\pi \rho_w} \right)^{1/3} \left( \frac{1}{\Delta N_h} + \frac{1}{\Delta N_g} - \frac{1}{\Delta N_c} \right)^{1/3} + \left( \frac{-6\rho q_i}{\pi \rho_i \Delta N_{ni}} \right)^{1/3} \right] + \left( \frac{6\Delta m_{ii}}{\pi \rho_i} \right)^{1/3} + K \frac{\partial^2 D_i}{\partial z^2}, \quad (4)$$

where PCC, PCI, PID, PII are, respectively, the condensation/evaporation rate onto/of cloud water droplets, the deposition/sublimation rate onto/of cloud ice crystals, the nucleation of water droplets, and the nucleation of ice crystals; PCS and PIS are, respectively, the sedimentation rate of cloud water droplets and ice crystals;  $N_h$  and  $N_g$  are, respectively, the number concentration

of cloud water droplets that freeze heterogeneously and homogeneously;  $N_c$  is the number concentration of water droplets or ice crystals that collide to form larger cloud particles;  $N_{nw}$  and  $N_{ni}$  are respectively, the number concentration of water droplets and ice crystals nucleated;  $m_{iw}$  and  $m_{ii}$  represents the mass of condensed/evaporated water and deposited/sublimated water, respectively;  $K$ ,

$\rho$ ,  $\rho_w$ ,  $\rho_i$ , and  $\Delta t$ , are, respectively, the eddy diffusion coefficient, air density, water density, ice crystal density, and model time step. Here  $\Delta$  indicates the variation of the variable during a time step ( $\Delta x = x_{t+\Delta t} - x_t$ ).

To compute the microphysical processes like condensation and aerosol activation, it is necessary to know the time evolution of the saturation ratio ( $S$ ). Unlike in most climate models that set a threshold for  $S$ , in this model  $S$  is free to evolve above the saturation point and depends on the total condensation/deposition rate and the atmospheric temperature cooling rate:

$$\frac{dS}{dt} = -\frac{L}{R_v T} \frac{dT}{dt} - \frac{p}{\varepsilon e_s} (\text{PCC} + \text{PCI} + \text{PID} + \text{PII}), \quad (5)$$

where  $R_v$ ,  $e_s$ ,  $p$ ,  $T$  are, respectively, the gas constant for water vapor, vapor partial pressure at water saturation, air pressure, and air temperature. Here  $\varepsilon = R_v/R_d$  where  $R_d$  is the gas constant for dry air. In this expression, variations of  $S$  associated with vertical velocity is included in the cooling rate term  $dT/dt$ . The LCM-NARCM model also simulates explicitly the aerosol size distribution. The model allows for several tracers and it is assumed that aerosols are internally mixed (Gong et al. 1997). The eleven size bins cover aerosol sizes ranging from 0.01 to 8  $\mu\text{m}$  in diameter. The following equation is used to predict the aerosol number concentration ( $N_{kl}$ ) for each tracer  $k$  in the size bin  $l$ :

$$\begin{aligned} \frac{\partial N_{kl}}{\partial t} + \mathbf{V} \cdot \nabla N_{kl} + \omega \frac{\partial N_{kl}}{\partial p} \\ = S_{\text{nucl}} + S_{\text{dep}} + S_{\text{wdep}} + \frac{N_a}{\Delta t}, \end{aligned} \quad (6)$$

where  $\mathbf{V}$  is the horizontal component of the wind and  $\omega$  is the vertical component of the wind expressed in  $\text{Pa s}^{-1}$ . Here  $S_{\text{nucl}}$ ,  $S_{\text{dep}}$ ,  $S_{\text{wdep}}$  represent, respectively, the nucleation of aerosols, dry, and wet deposition and are described in detail in Gong et al. (1997);  $N_a$  is the aerosol number concentration that is activated to form either water droplets or ice crystals. The advection terms on the left-hand side are provided through the RIM using local observations at the point of interest. In our case, we used the observation at Alert. Weekly mean aerosol concentrations at the surface are available from the climate archive. We assumed a constant aerosol concentration in the vertical from the surface to 5 km and during the week. This assumption may appear in contradiction with several observations that indicate important variations in the vertical (e.g., Barrie 1986). However, there is no common denominator between observations with regard to the variation of aerosol concentration with height. It generally depends on the presence of clouds and on the air layer origin, which vary as a function of height. Consequently, it is a simpler and unambiguous choice to assume a uniform vertical structure in the absence of measurements.

Equations (1)–(6), along with the traditional dynamical equations (continuity equation, thermodynamic equation,

hydrostatic equation, and momentum equation) form the system of prognostic equations used in the LCM-NARCM model. In the next section, a description of the parameterization developed to represent the microphysical processes present in Eqs. (1)–(6) is presented.

### c. Microphysical processes

Most of the microphysical processes influencing ice crystals depend on the ice crystal shape and density. Consequently, in order to parameterize the physical processes involving ice crystals, one has to characterize the ice crystal shape. As opposed to water droplets, ice crystals have different shape and density depending on the temperature and supersaturation (Pruppacher and Klett 1997). A large variety of crystal habits have been observed in the Arctic (Bigg 1980) [see Curry et al. (1990) for a comprehensive review]. However, laboratory experiments and observations have shown that column and needle crystal shapes seem to dominate at the cold temperatures and high relative humidities characteristic of the arctic winter (Bigg 1980; Pruppacher and Klett 1997). Given 1) the extreme complexity of developing an ice cloud parameterization accounting for several crystal habits and 2) the very limited knowledge and uncertainty prevailing in this field, the problem is simplified by assuming a single crystal shape. A column-needle shape is assumed in our simulation with a length/radius ratio of 10. Although somewhat arbitrary, this ratio agrees with several observations over the Arctic Ocean during winter (Bigg 1980). Also, this crystal shape seems to be predominant in very low temperatures and in polluted air mass characteristics of the Arctic during winter (Barrie 1986; Meyers and Hallett 1998).

#### 1) PARAMETERIZATION OF COLLISION PROCESSES

Collision processes include aggregation of ice crystals, coalescence of water droplets, and accretion of water droplets onto ice crystals. The collision process can be adequately described by the stochastic collection theory (Cotton and Anthes 1989); however, it is not realistic to include such a complex equation in a climate model. A parameterization of the collision processes is required. Few attempts have been made by cloud physicists to parameterize this process. Existing parameterizations depend on the cloud water and ice content and the temperature and assume a Marshall–Palmer size distribution of cloud particles (Cotton and Anthes 1989). Further they do not account for the variation of the collision rate within long time steps found in climate models.

In this work, we used two parameterizations to simulate the collision between cloud particles. The first one is the method of moments developed by Eneukashvili (see Pruppacher and Klett 1997). This parameterization is derived by writing the stochastic coalescence equation in terms of the moments of cloud particle number con-

centration. The equation is then resolved for a constant collection efficiency, which represents a population of particles within the Stokes flow regime, below  $50 \mu\text{m}$ . The decreasing rate of cloud particles through collisions is then given by

$$\frac{\Delta N_c}{\Delta t} = \min \left[ \varepsilon (-7.67 \times 10^5) q^{4/3} N_c^{2/3}, \frac{N_c}{\Delta t} \right], \quad (7)$$

where  $q$  and  $N_c$  are either the cloud ice or water mixing ratio and the number concentration of water droplets or ice crystals, respectively. Here  $\varepsilon$  is a factor that allows for aggregation by reducing the collection efficiency. Based on several laboratory experiments (Pruppacher and Klett 1997), we have fixed  $\varepsilon$  to 0.1, meaning the collection efficiency is a factor of ten smaller than the collection efficiency for water droplets.

Figure 1 shows the relative error produced by this parameterization when compared to the reference model for simulations of 20 min with different ice crystal concentrations. At ice water contents less than or equal to  $0.01 \text{ g m}^{-3}$ , errors are negligible. On the other hand, at larger concentrations, the errors grow very rapidly with increasing mean diameter. This is due to the variations in the collision rate during the typical climate model time step of 20 min. At large concentrations and large mean diameters, the collision rate is high and number concentration of ice particles decreases very rapidly. This leads rapidly to important variations in the collision rate. Neglecting this variation overestimates the collision rate.

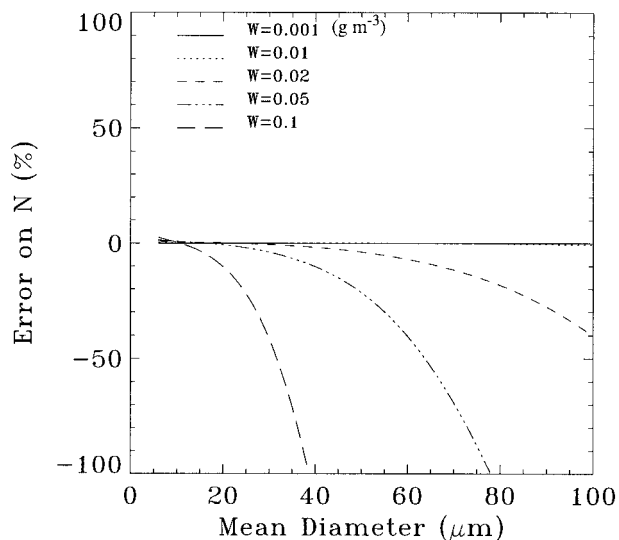


FIG. 1. Relative error produced on the total aerosol number after a 20-min simulation for five different ice water contents when the method of moment [Eq. (7)] is used to calculate the aerosol coagulation rate. Note that during these simulations, only the coagulation is allowed for, all other aerosol microphysical processes are omitted.

To avoid this error, we used the reference model of GB2001 as a tool to parameterize the collision rate at ice water content exceeding  $0.01 \text{ g m}^{-3}$ . The following expression has been developed:

$$\frac{\Delta N_c}{\Delta t} = \min \left[ \exp \left( \varepsilon \left\{ E(\log(D)) + G(D) \log \left[ \left( \frac{\rho W}{W_{\text{REF}}} \right) + \log \left( \frac{\sigma_{\text{REF}}}{\sigma} \right) \right] \right\} \right), \frac{N_c}{\Delta t} \right], \quad (8)$$

where  $W_{\text{REF}}$  and  $\sigma_{\text{REF}}$  are constants,  $\sigma$  is the standard deviation of the cloud particle size distribution,  $W$  is the cloud water content (ice or liquid), and  $E$  and  $G$  are polynomial expressions of degree four. Their coefficients are given in the appendix. Figure 2 shows the relative error produced by the parameterization compared to the reference model after one 20-min time step. For mean diameters of cloud particles less than  $30 \mu\text{m}$ , typical of ice fogs or stratus, the error is less than 10%. For larger mean diameters, the errors are substantial when the cloud water and ice content is larger than  $0.02 \text{ g m}^{-3}$ . However, at these diameters typical of diamond dust event, simulations with explicit microphysics GB2001 model and observations (Curry et al. 1996) have shown that the ice water content is usually below  $0.02 \text{ g m}^{-3}$ . Within these limits, the parameterization based on (7) and (8) can be used for the arctic winter low clouds with an error below 10%. In view of other uncertainties, this limit is considered acceptable for the time being.

## 2) PARAMETERIZATION OF CONDENSATION DEPOSITION

The total condensation/deposition rate  $C = \Delta m_{iw} + \Delta m_{ii}$  of water vapor onto ice crystals, water droplets, and aerosol nuclei is given by the following theoretical expression:

$$\begin{aligned} C = & \int_{D_a} \left[ \int_{\delta'} n(\delta') d\delta' \right] \frac{d}{dt} m(D_a) dD_a \\ & + \int_{D_w} n(D_w) \frac{d}{dt} m(D_w) dD_w \\ & + \int_{D_i} n(D_i) \frac{d}{dt} m(D_i) dD_i, \end{aligned} \quad (9)$$

where the first term of the right-hand side is the condensation/deposition rate onto activating aerosols

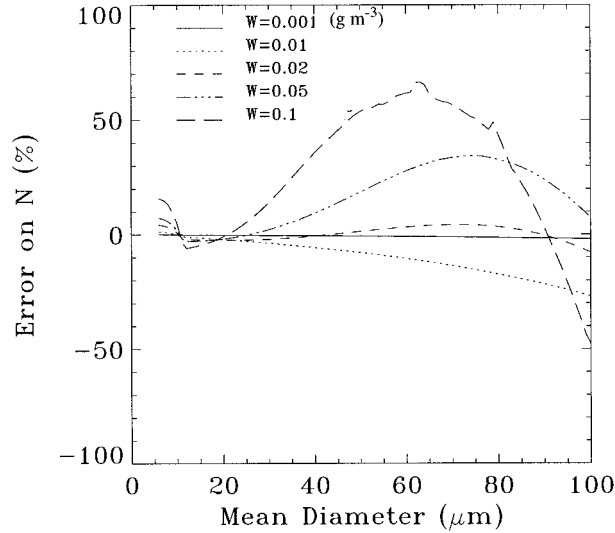


FIG. 2. Relative error produced on the total aerosol number after a 20-min simulation for five different ice water contents when the parameterization of coagulation based on the reference model [Eq. (8)] is used to calculate the aerosol coagulation rate. Note that during these simulations, only the coagulation is allowed for, all other aerosol microphysical processes are omitted.

[terms PII and PCI in Eqs. (1), (2), and (6)] and the second and third terms are the condensation rate onto preexisting water droplets (term PCC) and deposition rate onto preexisting ice crystals (term PID), respectively. The first term depends on the number of activated aerosols and is found by the methods described in the next two sections. The second term on the right-hand side of Eq. (9) has been parameterized using a method similar to Cotton et al. (1982). Given  $N_w$  cloud droplets ( $m^{-3}$ ) and  $N_i$  cloud ice crystals ( $m^{-3}$ ) of mean diameter  $D_w$  and  $D_i$ , respectively, the total condensation and deposition rate on cloud water droplets (PCC) and ice crystals (PID) is given by the following expressions:

$$\begin{aligned} \text{PCC} &= \int_{D_w} n(D_w) \frac{d}{dt} m(D_w) dD_w \\ &\approx \min \backslash \max \left[ N_w \frac{d}{dt} m(D_w) \alpha(N_w, D_w) \eta, \frac{q_w - q_{sw}}{\Delta t} \right], \end{aligned} \quad (10)$$

$$\begin{aligned} \text{PID} &= \int_{D_i} n(D_i) \frac{d}{dt} m(D_i) dD_i \\ &\approx \min \backslash \max \left[ N_i \frac{d}{dt} m(D_i) \alpha(N_i, D_i) \eta, \frac{q_i - q_{si}}{\Delta t} \right], \end{aligned} \quad (11)$$

where the minimum function is applied in case of supersaturated air whereas the maximum function is applied in case of subsaturated air,  $q_{sw}$  and  $q_{si}$  are the

saturation vapor pressure with respect to water and ice, respectively,  $\eta$  is a correction factor necessary to compensate the systematic underestimation of this expression of the total condensation rate due to the assumed cloud lognormal size distribution. This factor depends on the dispersion of the size distribution. In this case, the correction factor equals 1.17 for a standard deviation of 1.4. Generally, climate models have time steps much longer than the microphysics timescale. The supersaturation is known at the beginning of the time step. However, between two time steps, it is expected to vary substantially in presence of cloud. Therefore, to obtain an average representative value for the time step, we added the relaxation factor  $\alpha$ . Although without real physical basis, this allows for proper treatment of other physical processes such as the aerosol activation where the condensation rate on cloud particles is a determining factor. The relaxation factor is based on the reference model described in GB2001 and expressed as

$$\alpha(N, D) = \frac{N}{N_{\text{ref}}} (aD + b), \quad (12)$$

where  $N_{\text{ref}}$ ,  $a$ , and  $b$  are constants (see appendix). The diffusional growth  $dm/dt$  in Eqs. (10) and (11) is approximated by using the mean diameter of cloud particles. In the case of deposition on ice crystals, the mean radius and length of the column crystal is calculated using  $D_i$  by assuming a ratio radius/length of 10. The capacitance that is used to calculate the deposition rate is found by using the approximation of Rogers and Yau (1989; GB2001). The saturation ratio, used to compute the diffusional growth, is the value at the beginning of the time step.

This parameterization was compared to the reference model for 20-min simulations. Figure 3 shows the resulting errors for different combinations of supersaturations and total number of cloud particles, representative of arctic low clouds during winter. Errors are negligible for low supersaturation typical of ice fog and stratus. At very high ice supersaturation and low total cloud particles, typical of diamond dust, the error is kept below 5%. The error increases with supersaturation and total cloud particles. However, observations indicate that conditions for large errors do not occur in ice fog, in stratus nor in diamond dust (Curry et al. 1990). For ice fog and stratus, the supersaturation is low and the cloud particle concentration is high, while in diamond dust, the opposite situation prevails.

In the current parameterization, we neglect the dependence of the condensation rate on pressure and temperature. As compared to the GB2001 explicit model, for pressure between 700 and 1000 hPa and temperature between 230 and 260 K, this approximation is responsible for less than 10% error. This temperature and pressure represents approximately the conditions under which low clouds form during winter in the Arctic. Fig-

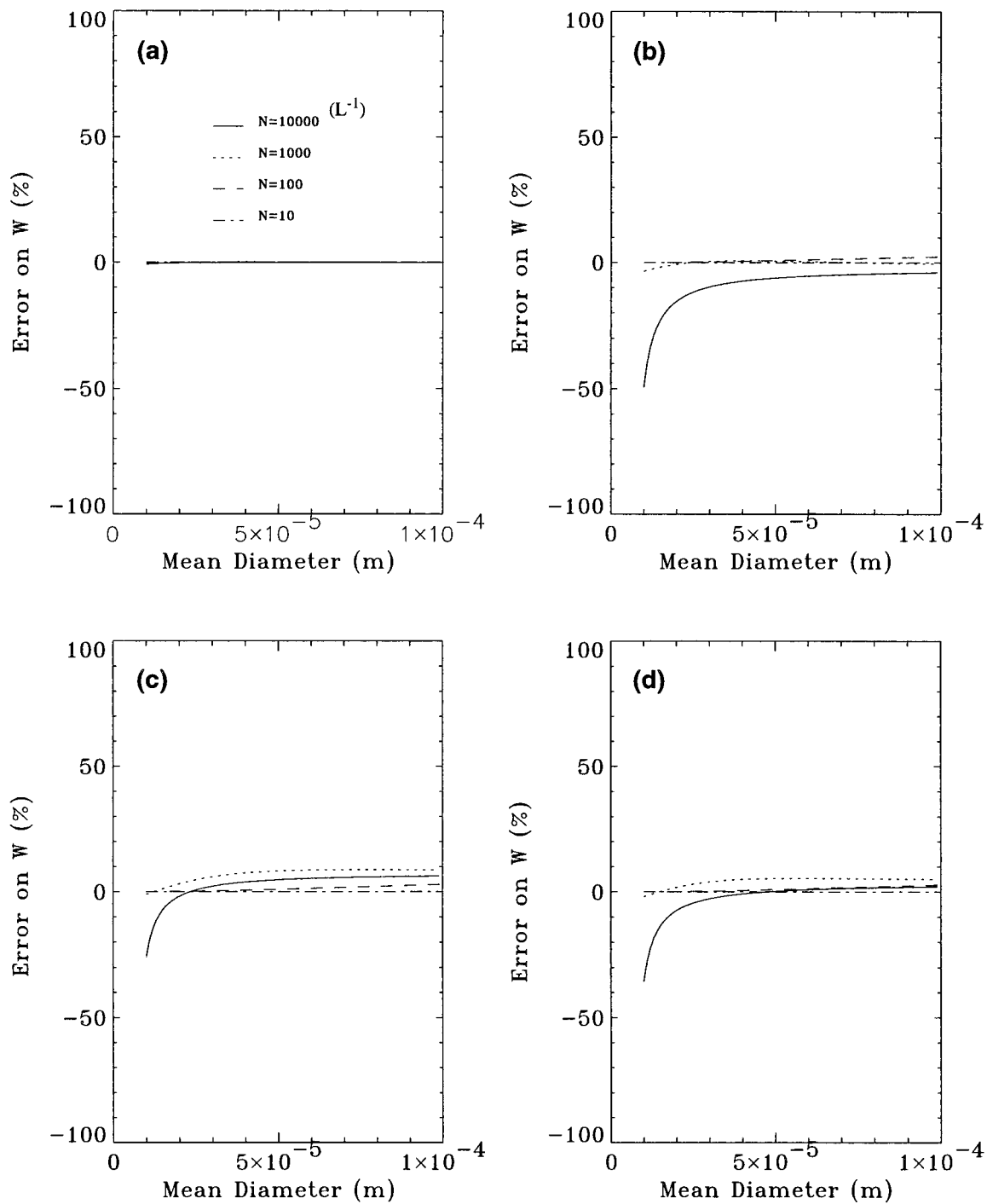


FIG. 3. Relative error produced on the ice water content after a 20-min simulation for four different ice crystal concentrations when the parameterization based on the reference model [Eq. (11)] is used to calculate the aerosol condensation rate. (a) Supersaturation is 0.5%,  $T = 240$  K, and  $P = 700$  hPa; (b)  $S = 30\%$ ,  $T = 240$  K, and  $P = 700$  hPa; (c)  $S = 30\%$ ,  $T = 240$  K, and  $P = 1000$  hPa; (d)  $S = 30\%$ ,  $T = 260$  K, and  $P = 700$  hPa. Note that during these simulations, only the condensation is allowed for, all other aerosol microphysical processes are omitted.



ure 3 shows the resulting error as a function of particle size.

### 3) AEROSOL ACTIVATION

The first term of Eq. (9) depends on the number of activated aerosols and the growth rate of activated aerosols. The aerosol growth rate is found by assuming a diameter of 10  $\mu\text{m}$ . That is based on the fact that an activated aerosol grows very rapidly between 1 and 10  $\mu\text{m}$  and its growth rate, in terms of diameter, decreases substantially afterward (Rogers and Yau 1989). For instance, a small water droplet of 0.9  $\mu\text{m}$  reaches a diameter of 10  $\mu\text{m}$  in less than 4 min. Given the 20-min time step of the model, we can reasonably approximate the droplet diameter at 10  $\mu\text{m}$ . Consequently, according to the diffusion growth theory, the condensation rate onto aerosol is approximated by the following relation in the model:

$$\frac{dm}{dt} = 0.0002\pi D_v \rho_{vs}(S - 1), \quad (13)$$

where the coefficient 0.0002 is the product  $4R$  with  $R = 5 \mu\text{m}$ . The activation of aerosols is driven by the supersaturation ( $S - 1$ ). Although the supersaturation is known at the beginning of the time step, its time variation within a time step is uncertain. It may increase or decrease monotonically during the period or it may reach a maximum and then decrease depending on the balance between production and condensation of water vapor. The evolution of supersaturation depends on the cloud particle number concentration and the cooling rate. But cloud particle number concentration varies with the supersaturation leading to an implicit problem where the unknown variable is present on both sides of the equation.

The method employed to find the number of activated nuclei within a time step is the following. Equation (5) can be written in the general form  $dS/dt = P - C$  (Rogers and Yau 1989), where  $P$ , a source term, is proportional to the cooling rate of the air and  $C$ , a sink term, represents the total condensation rate and is given by Eq. (9). The first step consists in assuming that no aerosol is activated during the climate model (CM) time step and to examine the temporal evolution of  $S$ . If  $dS/dt$  is negative, then  $S$  decreases and no aerosol is activated. This situation corresponds either to a warming of the atmosphere (term  $P$  negative) or to a depletion by existing ice crystals absorbing excessed water vapor more rapidly than produced by cooling.

On the other hand, if  $S$  increases with time, two situations can arise:  $S$  can either increase during the entire CM time step or reach a maximum and then decrease. To find out what situation occurs within a given time step, we first compute the theoretical maximum saturation by setting  $dS/dt = 0$  and by isolating  $n(r)dr$  in the first term of the right-hand side of Eq. (9). This value of  $n(r)dr$ , which we call  $n_1$ , represents the number

of activated aerosols if saturation reached its maximum value within a CM time step. Another value of  $n(r)dr$ ,  $n_2$ , is calculated by assuming a constant value of  $dS/dt$  (corresponding to its value at the beginning of the CM time step) throughout the CM time step. If  $n_2 > n_1$ , then saturation has necessarily reached a maximum during the CM time step, and consequently, the number of activated aerosols is  $n_1$ . On the other hand, if  $n_1 > n_2$ , the maximum number of activated aerosols is set to  $n_2$ . Then, the real number of activated aerosols corresponds to the concentration of CN/IN greater than the critical diameter of activation. This number must be smaller than or equal to the value calculated previously, that is either  $n_2$  or  $n_1$ .

At this point, the *potential* number of activated aerosols can be evaluated. However, this number should be consistent with the number of available CN or IN. For instance, if  $n = n_1$ , the saturation has reached its maximum and the critical radius of activation  $r_c$  can be estimated. By integrating over the radius range larger than  $r_c$  we obtain the number of activated aerosols,  $n_a$ . The value of  $n$  is then limited by  $n_a$ , which depends essentially on aerosol spectrum and to a lesser extent on aerosol composition. With an explicit aerosol scheme, such as in the LCM and NARCM,  $n_a$  is found by adding aerosols in size bins larger than the critical diameter of activation. The next section describes a method for calculating  $n_a$  without an explicit representation of the aerosol spectrum.

After activation, we assume in this parameterization that the resulting cloud particle size distribution is log-normal, monomodal in the case of one phase or bimodal in the case of mixed phase, with a standard deviation of 1.4. The mean diameter depends on whether there are preexisting cloud particles or not. In the case without precursor, the mean diameter is simply calculated according to the available condensable water and the number of activated nuclei. Otherwise, the dominant spectrum in terms of number concentration, either the newly activated cloud particles or the preexisting cloud particles dominates.

### 4) ALTERNATIVE TO THE EXPLICIT AEROSOL REPRESENTATION

An explicit size-segregated aerosol spectrum simulation, as in NARCM-LCM, provides a prognostic evaluation of  $n_a$ . However, most climate models consider only the bulk of aerosol mass. In this case, the method developed by Khvorostyanov and Curry (1999, hereafter referred to as the KC method) is used. The KC method assumes implicitly a power-law type of aerosol distribution. A theoretical expression is then derived for the aerosol size distribution  $f(r)$  as a function of humidity, aerosol solubility, and composition as follows:

$$f(r) = Nr_{\min}^{\mu-1} (2R) \left(\frac{b}{B}\right)^R r^{(\mu+\beta)(1+\beta)} \quad \text{for } H > 0.95, \quad (14)$$

$$f(r) = 3Nr_{\min}^{\mu-1} \left(\frac{b}{1-H}\right)^R R \left[ r^{\mu_{\text{wet}}} - \left(R + \frac{1}{3}\right) \frac{B}{(1-H)} r^{-(\mu_{\text{wet}}+1)} \right] \quad \text{for } H < 0.95, \quad (15)$$

where  $R$  and  $\mu_{\text{wet}}$  are function of  $\mu$  and  $\beta$  (see KC 1999),  $\mu$  is the slope of the Junge size distribution,  $H$  is the saturation ratio,  $r_{\min}$  is the lower limit radius of the aerosol size distribution, and  $b$  and  $\beta$  depends on aerosol composition (see KC 1999). One obtains the total number of activated aerosols by integrating these expressions from the critical radius of activation to the infinity.

To assess this method, a 20-day simulation has been performed and compared to the NARCM–LCM explicit aerosol scheme. The period from 1 to 20 January 1991 at Alert is used. Temperature, humidity, and aerosol concentration are obtained from observation data throughout the period. Aerosols are assumed to be mostly sulfuric acid with 90% of the aerosol volume being soluble. For the simulation with the KC method, the small end of the aerosol spectrum ( $r_{\min}$ ) is set to 0.1  $\mu\text{m}$ . In the explicit scheme simulation, the aerosol spectrum is a superposition of two lognormal distributions centered, respectively, at 0.1 and 0.6  $\mu\text{m}$ . Sea salt and soil particles form the larger mode while other components such as sulfate and carbonaceous particles form the smaller mode.

Figure 4 shows the number of activated aerosols in the lowest model level for three aerosol distribution slopes. The KC method is in good agreement with the detailed scheme for  $\mu = 2.5$ . Higher slopes lead to increasing underestimation of the number of activated aerosols, mainly during the second episode, that is days 12–20. Two distinct periods can be distinguished: days 0–12 with low number of activated aerosols and days 13–20 during which the number of activated aerosols is high with values ranging from  $10^6$  to  $10^8 \text{ m}^{-3}$ . The first period corresponds to a situation of boundary layer diamond dust while the second period is characterized by the formation of a thin stratus cloud at 800 hPa. In the diamond dust case (days 0–12), the results are insensitive to the slope of the aerosol distribution. In this case, most of the time  $n_a$  is much higher than the number of ice nuclei. Therefore, even if  $n_a$  differs greatly from the value calculated with the explicit scheme, it is limited by the ice nuclei concentration and becomes insensitive to  $\mu$ . However, in the stratus case, temperature is much lower and the IN concentration is higher. As a result,  $n_a$  is often lower than the IN concentration and consequently, it is not limited by the IN concentration anymore. The real number of activated aerosols in these situations is then given by  $n_a$ . Figure 4 shows that the slope 2.5 is the most suitable choice as compared to the explicit scheme.

A slope of 2.5 may appear somewhat surprising since slopes varying between 3.0 and 4.0 are usually reported in the literature (Pruppacher and Klett 1997). At 0.05–0.1- $\mu\text{m}$  radius, which corresponds to the modal radius range of the aerosol size distribution, the slope decreases dramatically to reach 0 at the maximum of the size

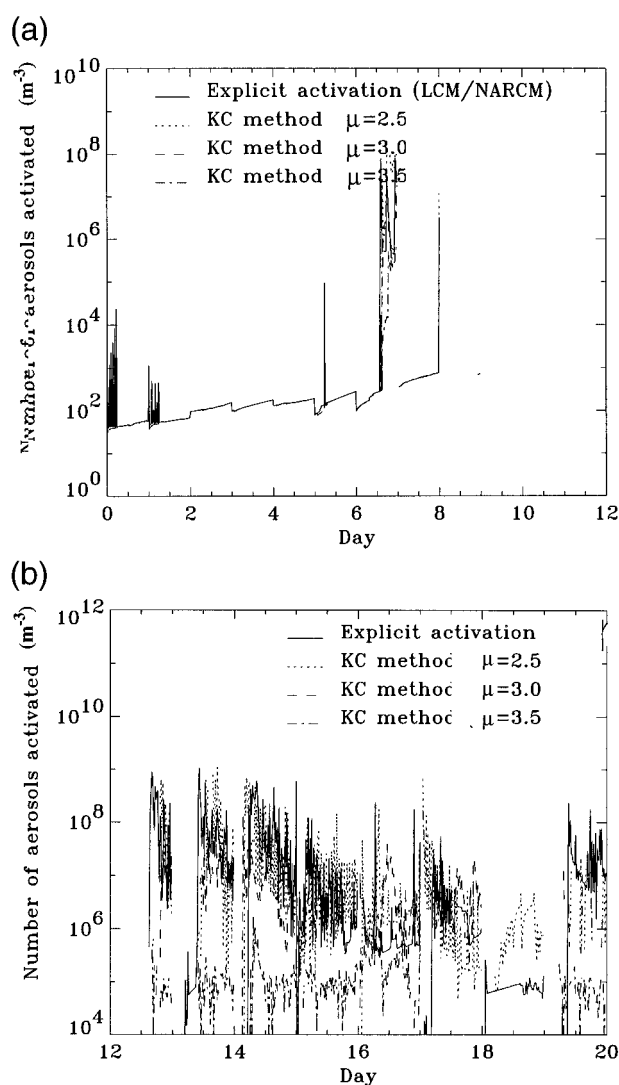


FIG. 4. Comparison between the temporal evolution of the number of activated aerosols obtained with the explicit aerosol scheme and the KC method used with three different aerosol slopes for (a) the first 12 days and (b) the last 8 days of the 20-day simulation with the LCM at 1000 hPa.

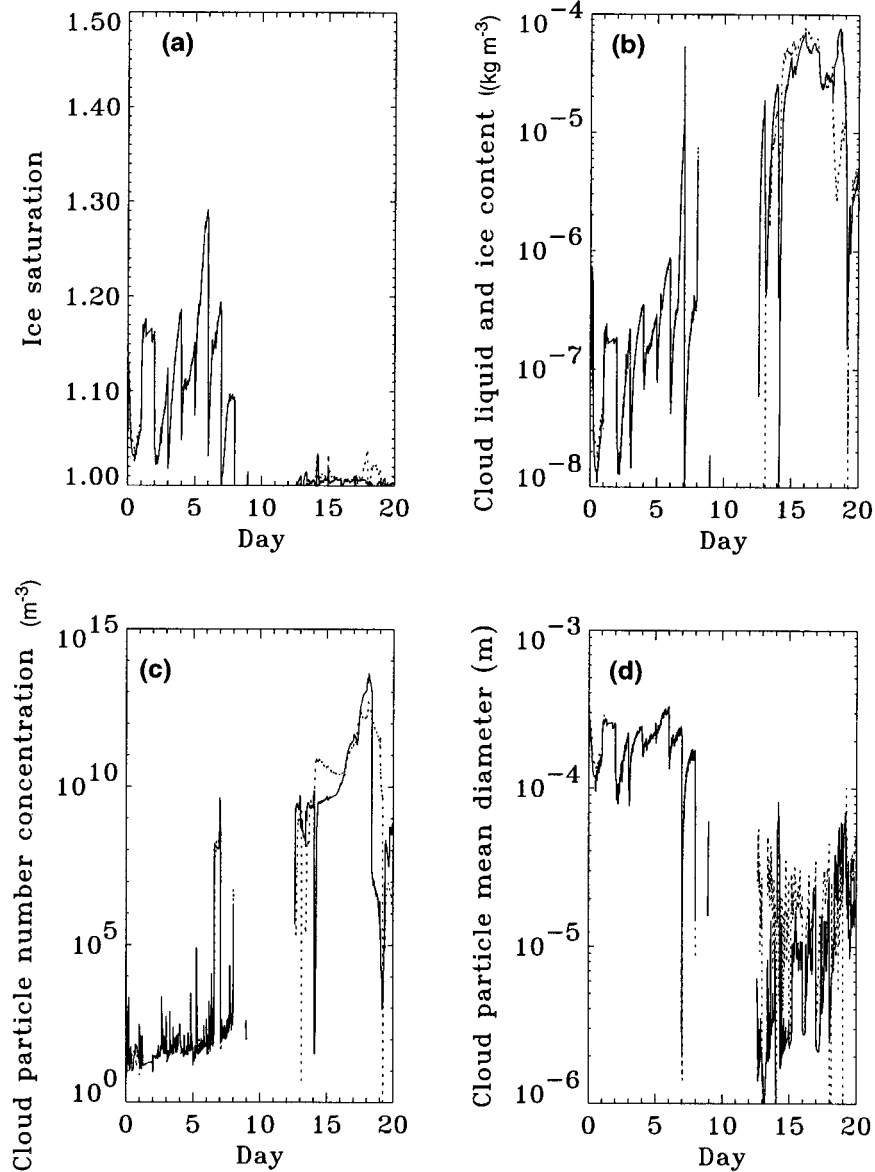


FIG. 5. Comparison between the temporal evolution of (a) the ice saturation, (b) the cloud liquid and ice content, (c) the cloud particle concentration, and (d) the cloud particle mean diameter obtained with the explicit aerosol scheme and the KC method used with an aerosol slope of 2.5 during the 20-day simulation with the LCM at 1000 hPa. Note that the very high cloud particle concentration between days 16 and 18 is due to high concentration of submicron water droplets (interstitial aerosols).

distribution. Therefore, the results obtained here indicate that the size of aerosols that contribute most to the formation of cloud particles is around  $0.1 \mu\text{m}$ . GB2001 have shown that this is due to the high supersaturation and the high frequency of activation, which does not allow for the formation of large aerosols between activation events.

Figure 5 shows the cloud ice content, ice crystal number concentration, ice saturation, and mean ice crystal diameter simulated with the slope 2.5 compared to the explicit scheme. The averaged value over the 20 days

for each field is shown in Table 2. The temporal evolution and the mean value of the saturation ratio, the cloud water and ice content, the mean cloud particle diameter, and the number of activated aerosols are reproduced by the KC method with less than 10% error. However the cloud particle number concentration is substantially underestimated. This is due to the condensation event on 18 January during which the KC method strongly overestimates the number of activated aerosols (see Fig. 4).

Despite its simplicity, the KC scheme is capable of

TABLE 2. Differences for averaged microphysics fields obtained during a 20-day LCM simulation with the explicit aerosol microphysics and with the Khvorostyanov and Curry (1999) (KC) method.

	LCM-NARCM aerosol explicit scheme	KC method ( $\mu = 2.5$ )	Difference (%)
Ice saturation	1.064	1.069	0.5
Cloud total water content ( $\text{Kg m}^{-3}$ )	$1.40 \times 10^{-5}$	$1.42 \times 10^{-5}$	1.2
Number concentration of cloud particles ( $\text{m}^{-3}$ ) (including submicron interstitial wet aerosols)	$8.33 \times 10^{11}$	$1.89 \times 10^{11}$	77.0
Mean diameter of cloud particles ( $\mu\text{m}$ )	106.2	114.2	7.5
Number of activated aerosols ( $\text{m}^{-3}$ )	$1.74 \times 10^7$	$1.92 \times 10^7$	10.0

reproducing with small errors the main microphysical variables used in the current parameterization. Therefore, to a first order, for arctic low-level clouds, the KC scheme is a good alternative to a size-segregated explicit aerosol scheme in a climate model.

### 5) GRAVITATIONAL DEPOSITION PARAMETERIZATION

To find the mass of precipitating cloud particles, we first assume that cloud particles are uniformly distributed in the volume bounded by the adjacent layers. If  $H$  is the height of the layer,  $V$  the mean velocity of the cloud particle distribution,  $t$  the time, and  $w$  the cloud water content, and  $i$  the ice content, then the mass rate of condensate ( $M_{kl}$ ) leaving the reference level  $k$  going to level  $l$  is then given by

$$M_{kl} = \text{PCS} + \text{PIS} = \frac{1}{H}(V_w q_w + V_i q_i). \quad (16)$$

The mass of cloud particles depositing to a layer below is assumed to be distributed uniformly in this layer. Further, the mean diameter of sedimenting particles is assumed to be the same of the arrival layer. This condition is required since, in the parameterization, the cloud particle size distribution is monomodal for each phase. In the case where there is no cloud in the arrival layer, we assumed it arbitrary that sedimenting particles have a mean diameter of  $100 \mu\text{m}$ .

The mean velocity of falling cloud particles has been parameterized as a function of  $D$  using the reference model MAEROS2 of GB2001. The terminal velocity of cloud particles is given by the following polynomial expression:

$$V_j = \frac{1}{f}(a_6 D_j^6 + a_5 D_j^5 + \dots + a_0), \quad (17)$$

where  $j$  stands for the phase,  $a_i$  are given in the appendix, and  $f$  is the shape factor taking into account the effect of cloud particle density and the ice crystal habit on the falling velocity. For a column type crystal with a length greater than  $28 \mu\text{m}$ , the shape factor follows the parameterization of Heymsfield (1972) as described in GB2001. In case of water droplets,  $f$  is set to 1.

### 6) ICE CRYSTAL NUCLEATION

Both homogeneous and heterogeneous ice nucleation are simulated in the model. The ice crystal nucleation is represented similarly as in the reference model of GB2001. The homogeneous nucleation of ice crystal is assumed to depend on temperature only. The homogeneous freezing temperature is either prescribed or can be parameterized as a function of the aerosol composition (see GB2001). For the heterogeneous nucleation, the model accounts for the temperature, the cooling rate, the saturation, and the water droplet size. The Bigg parameterization (Pruppacher and Klett 1997) allows for determining the median freezing temperature of population of water droplets as a function of mean particle size. To take into account the supersaturation and temperature, the parameterization of Meyers et al. (1992) is used.

In practice, we use the Bigg parameterization to determine the critical diameter of freezing ( $D_f$ ) at which water droplets may freeze. The number of water droplets greater or equal to this size that freeze is then limited by the number of available IN given by the parameterization of Meyers et al. (1992). Since the liquid water content and the mean diameter of water droplet are prognostic quantities, we use this along with the assumption of a lognormal size distribution of standard deviation of 1.4 to calculate the number of water droplets of diameter larger than  $D_f$  as follows:

$$N_H = \int_{D_f}^{\infty} \frac{N_w}{(2\pi)^{1/2} \ln \sigma} \exp\left[-\frac{\ln(D - \ln D_w)^2}{2(\ln \sigma)^2}\right] dD. \quad (18)$$

### 3. Validation with the reference model

The parameterization presented in the previous section has been assessed with the reference model of GB2001 and compared against observations at Alert for the period 1991–94. Figure 6 shows a comparison between the parameterization and the reference model for 12 h simulation of the formation of ice crystal during an atmospheric isobaric cooling of  $2 \text{ K day}^{-1}$  at 980 hPa. The ice crystal mass concentration has been chosen to make the comparison since 1) every microphysical process parameterized alter this field and 2) this is the most important microphysical variable in a climate

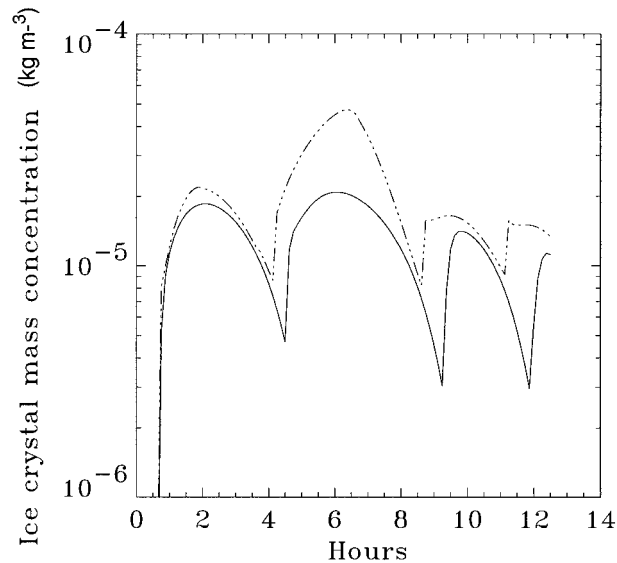


FIG. 6. Comparison between the reference model and the parameterization when all microphysical processes are taken into account for a 12-h simulation of the formation of ice crystals during an atmospheric isobaric cooling of  $2 \text{ K day}^{-1}$  at 980 hPa.

model. In these simulations, the only difference is the microphysical treatment, everything else being the same. The maximums at hours 2, 6, 10, and 13 correspond to the activation of many condensation or ice forming nuclei. The following concentration collapses are due to the combined effect of ice crystal aggregation and sedimentation.

The parameterization shows a good agreement with the ice crystal mass concentration variation. However, the scheme seems to systematically overestimate the ice crystal mass concentration. The error is sometimes substantial as illustrated at hour six. At that time, the ice crystal mass concentration is overpredicted by a factor two. Also, the parameterization greatly overestimates the minima. However, it captures the main features of the temporal evolution of ice crystal concentration.

Besides the intrinsic errors due to the parameterization itself, two main sources of errors have been identified: the assumption made on the cloud particle size distribution mean diameter after activation of aerosols and after the gravitational settling of larger particles coming from upper layers. The model underestimates the mean cloud particle diameter due to the monomodal size distribution assumption on cloud water droplets and ice crystals.

The error produced by the monomodal size distribution assumption was assessed by comparing the reference model with the parameterization for 2-days simulation of an air column radiative cooling. Both microphysics schemes were incorporated into simple column radiative model (see GB2001) for this experiment. Since ice crystals are a major absorber of IR radiation, the goal of this test was to evaluate the error on the surface

cooling produced by the parameterization. Surface cooling was found to be underestimated by 15%. Given the existing time constraint in climate model parameterizations, this error remains acceptable in that context.

#### 4. Case of Alert

The LCM-NARCM model has been used to simulate the case of Alert from January 1991 to May 1991, November 1991 to May 1992, November 1992 to May 1993, and November 1993 to April 1994. Aerological soundings and aerosol observations served to drive the model. Thus, the model allows for temperature advection, humidity advection, and momentum advection.

Aerosol weekly mean observations have been provided by the Alert laboratory station located 6 km south of the main base on an elevated plateau 210 m above sea level (Sirois and Barrie 1999). Data are taken at the screen level. Eighteen ions, for which  $\text{SO}_4^-$ ,  $\text{NH}_4^+$ ,  $\text{H}^+$ ,  $\text{Na}^+$ ,  $\text{Cl}^-$  are the main elements, were collected on 20 by 25 cm Whatman 41 filters using a high volume sampler.

In the model, we consider two aerosol modes, the accumulation mode and the giant particle mode centered at 0.17 and 0.6  $\mu\text{m}$ , respectively. Size distributions are lognormal with standard deviations of 1.42 and 2.01 for the accumulation and giant mode, respectively. These parameters were used by Blanchet and List (1983) based on observations of Heintzenberg (1980) and Bigg (1980). This approximation is a good representation of many other aerosol spectra observed in the Arctic (Hoff et al. 1983; Radke et al. 1989). These conditions are applied in the assimilation run that allows for calculation of the dynamic tendencies associated to the aerosols. In the simulation run, the aerosol spectrum is free to change.

We assumed that the giant mode is formed by sea salt aerosols (Na, Cl, Mg, etc.) and soil particles (Si, Al, etc.). Other ions have been assumed to be part of the accumulation mode. This approximation somewhat underestimates the giant mode since sea salt aerosols contain sulfate (Bigg 1980; Sirois and Barrie 1999). However, observations show that sulfate proportion in sea salt aerosol is small (Sirois and Barrie 1999). Besides these components, organics and black carbon have been added in proportion of sulfate mass since these components have not been measured at the station. Since both organics and black carbon come mostly from anthropogenic sources (Heintzenberg and Covert 1987), their mass has been arbitrarily fixed to, respectively, 20% and 5% of the total mass of sulfate. These values reflect observations taken in the Arctic during winter (Barrie 1986).

In the simulations, thermodynamical and physical properties of aerosols are prescribed initially and do not depend on the real observed composition. The observations are used only to drive the model for the aerosol mass in each mode of the bimodal size distribution. This

TABLE 3. Three characteristics distinguishing both aerosol scenarios for the LCM simulations.

	Scenario 1	Scenario 2
Solubility	50%	100%
Homogeneous freezing temperature	238 K	Bertram et al. (1996)
Ice forming nuclei concentration	Meyers et al. (1992)	Meyers et al. (1992)/100

technique simplifies the determination of the aerosol microphysical properties. Further, it allows sensitivity tests to be performed by comparing different aerosol scenarios.

Two aerosol scenarios have been compared in our experiment: 1) a natural background aerosol population and 2) an acidic aerosol population typical of the Arctic haze events. Acidic aerosols are distinguished from natural background aerosol by the anthropogenic sulfate mass that may increase 10 times the background value (Bridgman et al. 1989). As a result, most of the aerosols contain sulfuric acid.

In our experiments, three characteristics of the acidic aerosols have been considered (see Table 3): 1) A larger solubility is associated with the acidic aerosols. Arbitrarily, the aerosol solubility has been fixed to 50% and 100% in scenarios 1 and 2, respectively. 2) A lower homogeneous freezing temperature of the acidic interstitial aerosols. Bertram et al. (1996) have shown that the homogeneous freezing temperature of an interstitial aerosol formed by a binary mixture of water and sulfuric acid depends on the proportion of sulfuric acid in the droplet. These laboratory experiments have been done for an ideal mixture and for droplets of  $0.1\text{-}\mu\text{m}$  of diameter. We have applied these results to the acidic aerosol scenario. For the natural background aerosol scenario, we assume a freezing temperature of 238 K, that corresponds approximately to the homogeneous freezing temperature of a pure water droplet. 3) The ice forming nuclei concentration, by which the heterogeneous ice nucleation can occur, is found with the parameterization of Meyers et al. (1992). It is lowered by a factor of 100 in the scenario 2, based on Borys (1989) measurements showing a substantial decrease from one to four orders of magnitude of the ice forming nuclei when sulfuric acid aerosol concentrations is higher, such as during Arctic haze events.

Figure 7 shows a comparison between the model and observations of the weekly mean frequency of precipitation over the period 1991–94 at Alert. Tables 4 and 5 present a more quantitative comparison in terms of average and correlation coefficient. Figure 7a shows that the model reproduces approximately the observation of the added weekly frequencies of diamond dust and ice fog (referred thereafter to as the total precipitation). Maxima at days 10, 30, and 140 as well as minima at day 20 and 130 are well reproduced. However, at other times the maxima and minima are often simulated one week earlier or later. As a result, the correlation coefficients for both scenarios are relatively weak; although scenario 2 is significantly positively correlated with the

observations. When the total precipitation is averaged over the entire period, scenario 2 with a value of 39% is very close to the observed value of 37%. The background natural aerosol scenario overestimates significantly the total precipitation frequency with an averaged value of 47%. In addition to the average, the variability of a variable is very important to simulate in a climate model. We compare the variability of the model for both scenarios with the observation. It turns out that both scenarios well reproduce the total precipitation variability with a standard deviation of 1.29 and 1.30 for the scenarios 1 and 2, respectively, compared to an observed value of 1.35. Therefore, in terms of mean and variability, the total precipitation frequency is well reproduced by the microphysics scheme.

Figures 7b and 7c show the same comparison for diamond dust only and ice fog only. Diamond dust is overestimated by the model whereas the ice fog is underestimated. This feature is more pronounced for the scenario 2 with a very low value for the ice fog frequency. This underestimation could be due in part to the assumption of a permanent ice-covered surface in the model. In reality, ice motion leads to ice cracks and open water. These situations are favorable to the ice fog formation. However, the acidic scenario (scenario 2) is better correlated with the observed frequency variations with a correlation coefficient of 0.35 compared to  $-0.10$  for the scenario 1 (see Table 3). It seems that the big maximum of ice fog frequency produced by the first scenario between days 45 and 90 artificially increases the mean value and is therefore not representative of the observations. Otherwise, the high value of the observed ice fog variability is well reproduced by both scenarios with standard deviation values of 1.87 and 2.10 for scenarios 1 and 2, respectively, compared to the observed value of 1.98.

The diamond dust mean weekly frequency is overestimated by both aerosol scenarios. However, the error is smaller for the scenario 2 (see Table 2). The modeled diamond dust is well correlated with observations, with coefficients of 0.30 and 0.40 for the scenarios 1 and 2, respectively. Further, both scenarios show good agreement with the diamond dust frequency variability, with standard deviation very close to the observation (see Table 4).

Although scenario 2 underestimates substantially the ice fog frequency, it is overall rather representative of the observations in terms of diamond dust mean frequency and also in terms of diamond dust and ice fog frequency temporal variations. This result is not sur-

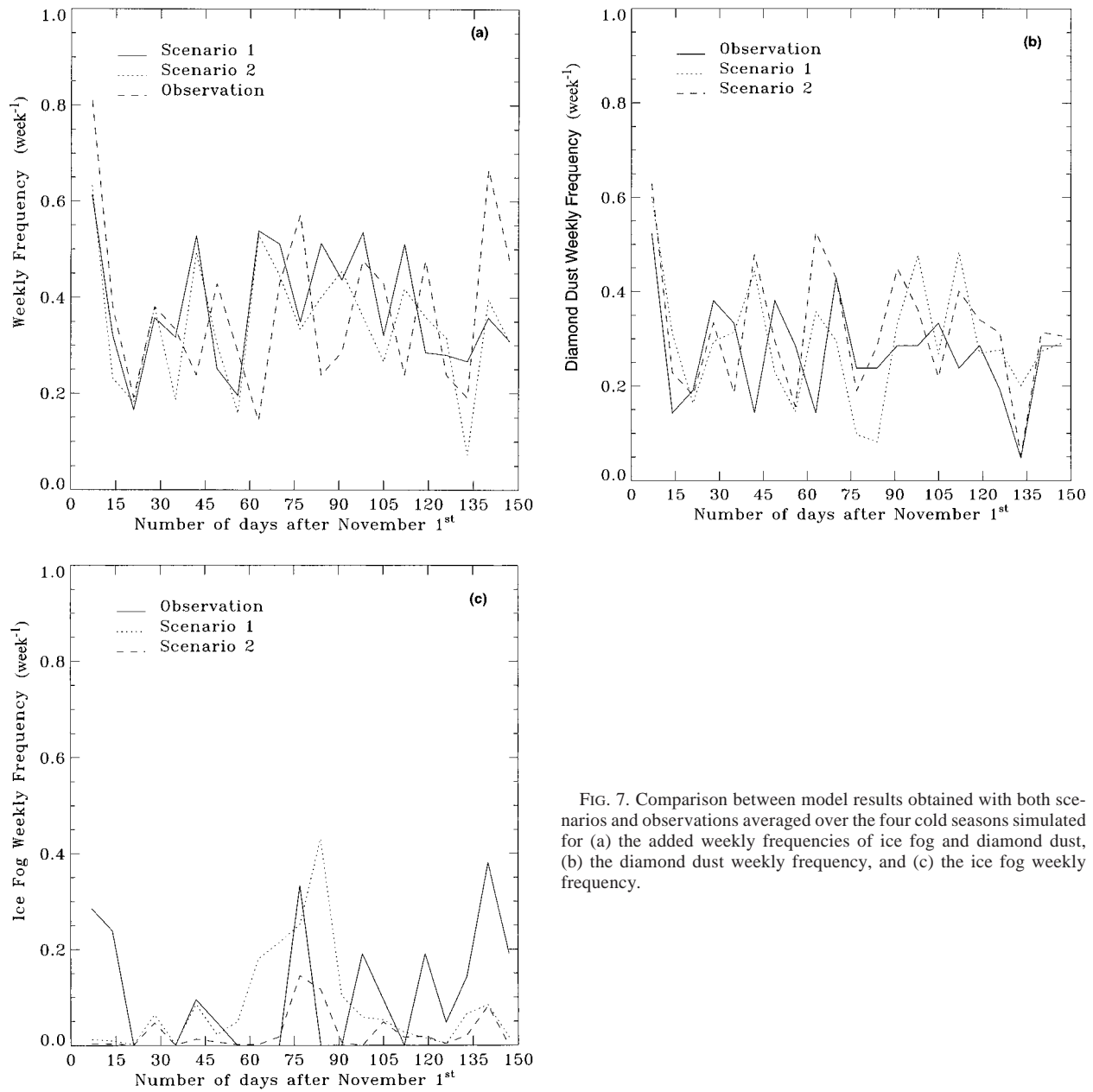


FIG. 7. Comparison between model results obtained with both scenarios and observations averaged over the four cold seasons simulated for (a) the added weekly frequencies of ice fog and diamond dust, (b) the diamond dust weekly frequency, and (c) the ice fog weekly frequency.

TABLE 4. Observed and modeled mean weekly frequency of ice fog and diamond dust averaged spatially in the vertical and averaged in time over the four cold seasons simulated. Standard deviations are also shown.

	Average			Standard deviation		
	Scenario 1	Scenario 2	Observation	Scenario 1	Scenario 2	Observation
Ice fog	10	4	11	1.87	2.10	1.98
Diamond dust	37	35	26	1.31	1.32	1.30
Total	47	39	37	1.29	1.30	1.35

TABLE 5. Correlation coefficient between observed and modeled ice fog and diamond dust weekly frequency temporal evolutions for the four cold seasons simulated for both scenarios.

	Scenario 1	Scenario 2
Ice fog	-0.10	0.35
Diamond dust	0.30	0.40
Total	0.18	0.35

prising since the aerosol population during this period contains high concentrations of sulfuric acid aerosols.

Except for errors associated with the parameterization itself, two sources of errors have been identified to explain the discrepancies between model results and observations. The first one is related to the climatological observations' accuracy and time resolution. As discussed in the introduction, the precipitation observation reliability is low due to the difficulties encountered in the detection of these phenomena (Curry et al. 1996). These factors might explain the model's tendency to overestimate the diamond dust. Further, the temporal and spatial resolution of the aerosol observation are low. As a result, vertical variability and short-term variability in the aerosol concentration are not allowed for in the model.

The second error source is related to the diagnostic determination of whether there is diamond dust or ice fog at a given time step or not. The method used to distinguish ice fog and diamond dust is highly subjective and may cause substantial errors. In the diagnostic method, if ice crystals have a diameter larger than  $30 \mu\text{m}$  and their number concentration is below  $100 \text{ L}^{-1}$ , the event is qualified as diamond dust. If these criteria are not satisfied, we assume it is an ice fog event. Furthermore, the ice crystals must be in the layer 900–1000 hPa. If it is the case, we assume that the observer has observed the ice crystals and reported it. This last assumption, which may appear somewhat exaggerated, has been set originally to counteract the parameterization tendency to underestimate the ice crystal sedimentation (see section 3). However, it could sometimes exaggerate the observed precipitation.

Ice crystals are often present in more than one layer. Then, an average of the ice crystal number concentration and diameter is done. Based on these averages, we applied the diagnostic method discussed above. However, this technique can lead to errors if ice crystal characteristics in one layer greatly differ from ice crystal characteristics of another level. The average values used in the diagnostic can then be nonrepresentative of the lower-tropospheric precipitation.

## 5. Conclusions

A new parameterization of ice crystal microphysics suitable for the arctic lower troposphere during winter has been presented in this paper. It can simulate, at low cost in a climate model, low-level ice clouds such as

thin stratus, ice fog, and diamond dust. The parameterization has been assessed against the modified detailed model MAEROS2. Comparisons have shown the ability of the parameterization to reproduce the main features of the ice crystal evolution during an air mass cooling. The parameterization has been included into the Canadian LCM–NARCM climate model. The model has been used to perform 4 yrs simulation at Alert. Comparisons with observations suggest that the LCM–NARCM can reproduce the mean and the variability of the added frequencies of diamond dust and ice fog during the cold season in the Arctic. However, it has problems distinguishing between precipitation type. Not surprisingly, the acidic aerosol scenario is more representative of the observations for the studied period.

Despite many approximations in the elaboration of this parameterization, it turns out that it can represent adequately, at low cost, the climatic mean and variability of the lower tropospheric precipitation in the Arctic during winter. Then, it will be possible to use the parameterization in 3D climate models to investigate indirect effects associated to the aerosols such as the dehydration–greenhouse feedback (Blanchet and Girard 1994, 1995).

*Acknowledgments.* The authors would like to thank Dr. Len A. Barrie for graciously providing the aerosol observations of the Alert meteorological station. We are also grateful for his useful comments and suggestions for this work. We also thank AES for support funding through the NARCM project.

## APPENDIX

### Quantitative Values of Constants Used in the Parameterization

Equation no.	Constants
(7)	$\epsilon = 0.1$ for ice crystals $\epsilon = 1.0$ for water droplets
(8)	$W_{\text{REF}} = 0.01 \text{ g m}^{-3}$ $\sigma_{\text{REF}} = 1.4$ $E(\log D) = \alpha_4 [(\log D)]^4 + \alpha_3 [(\log D)]^3 + \dots + \alpha_0$ $a_4 = 0.4224406$ $a_1 = 7.0921296$ $a_3 = 2.4431637$ $a_0 = 7.0314812$ $a_2 = 5.3237574$ $G(D) = (b_4 D^4 + b_3 D^3 + \dots + b_0 \log(W/W_{\text{REF}}))$ $b_4 = -7.2291528 \times 10^{-9}$ $b_1 = -0.014768$ $b_3 = 1.185372 \times 10^{-6}$ $b_0 = 2.057122$ $b_2 = 2.389730 \times 10^{-5}$
(12)	$N_{\text{ref}} = 1000 \text{ L}^{-1}$ $a = 8401981.1$ $b = -60.697$
(16)	$a_6 = -0.368703$ $a_2 = -3.273465 \times 10^{-6}$ $a_5 = 0.120703$ $a_1 = 1.667883 \times 10^{-8}$ $a_4 = 0.005990$ $a_0 = 3.097547 \times 10^{-11}$ $a_3 = 0.000265$



## REFERENCES

- Barrie, L. A., 1986: Arctic air pollution: An overview of current knowledge. *Atmos. Environ.*, **20**, 643–663.
- Beesley, J. A., and R. E. Moritz, 1999: Toward an explanation of the annual cycle of cloudiness over the Arctic Ocean. *J. Climate*, **12**, 395–415.
- Benson, C. S., 1970: Ice fog. *Weather*, **25**, 11–18.
- Bertram, A. K., D. D. Patterson, and J. J. Sloan, 1996: Mechanisms and temperature for the freezing of sulphuric acid aerosols measured by FTIR extinction spectroscopy. *J. Phys. Chem.*, **100**, 2376–2383.
- Bigg, E. K., 1980: Comparison of aerosol at four baseline atmospheric monitoring stations. *J. Appl. Meteor.*, **19**, 521–533.
- Blanchet, J.-P., and R. List, 1983: Estimation of optical properties of Arctic haze using a numerical model. *Atmos.–Ocean*, **21**, 444–465.
- , and E. Girard, 1994: Arctic greenhouse cooling. *Nature*, **371**, 383.
- , and —, 1995: Water-vapor temperature feedback in the formation of continental Arctic air: Implications for climate. *Sci. Total Environ.*, **160/161**, 793–802.
- Borys, R. D., 1989: Studies of ice nucleation by arctic aerosols on AGASP-II. *J. Atmos. Chem.*, **9**, 169–185.
- Boville, B. A., and P. R. Gent, 1998: The NCAR Climate System Model, version one. *J. Climate*, **11**, 1115–1130.
- Bridgman, H. A., R. C. Schnell, J. D. Kahl, G. A. Herbert, and E. Joranger, 1989: A major haze event near Point Barrow, Alaska: Analysis of probable source regions and transport pathways. *Atmos. Environ.*, **23**, 1–13.
- Briegleb, B. P., and D. H. Bromwich, 1998: Polar radiation budgets of the NCAR CCM3. *J. Climate*, **11**, 1246–1269.
- Bromwich, D. A., 1988: Snowfall in high southern latitudes. *Rev. Geophys.*, **26**, 149–168.
- Caya, D., and R. Laprise, 1999: A semi-implicit semi-Lagrangian regional climate model: The Canadian RCM. *Mon. Wea. Rev.*, **127**, 341–362.
- Considine, G., and J. A. Curry, 1996: A statistical model of drop-size spectra for stratocumulus clouds. *Quart. J. Roy. Meteor. Soc.*, **122**, 611–634.
- Cotton, W. R., and R. A. Anthes, 1989: *Storm and Cloud Dynamics*. Academic Press, 883 pp.
- , M. A. Stephens, T. Nehr Korn, and G. J. Tripoli, 1982: The Colorado State University three-dimensional cloud/mesoscale model-1982. Part II: An ice-phase parameterization. *J. Rech. Atmos.*, **16**, 295–320.
- Curry, J. A., 1983: On the formation of continental polar air. *J. Atmos. Sci.*, **40**, 2278–2292.
- , and E. E. Ebert, 1990: Sensitivity of the thickness of Arctic sea ice to the optical properties of clouds. *Ann. Glaciol.*, **14**, 43–46.
- , F. G. Meyers, L. F. Radke, C. A. Brock, and E. E. Ebert, 1990: Occurrence and characteristics of lower tropospheric ice crystals in the Arctic. *Int. J. Climatol.*, **10**, 749–764.
- , W. B. Rossow, D. Randall, and J. L. Schramm, 1996: Overview of Arctic cloud and radiation characteristics. *J. Climate*, **9**, 1731–1764.
- Fowler, L. D., D. A. Randall, and S. A. Rutledge, 1996: Liquid and ice cloud microphysics in the CSU General Circulation Model. Part I: Model description and simulated microphysical processes. *J. Climate*, **9**, 489–529.
- Gelbard, F., Y. Tambour, and J. H. Seinfeld, 1980: Simulation of multicomponent aerosol dynamics. *J. Colloid Interface Sci.*, **78**, 485–501.
- Ghan, S. J., and R. C. Easter, 1992: Computationally efficient approximation to stratiform cloud microphysics parameterization. *Mon. Wea. Rev.*, **120**, 1572–1582.
- Girard, E., and J.-P. Blanchet, 2001: Simulation of Arctic diamond dust, ice fog, and thin stratus using an explicit aerosol–cloud–radiation model. *J. Atmos. Sci.*, **58**, 1199–1221.
- Gong, S. L., L. A. Barrie, and J.-P. Blanchet, 1997: Modelling sea-salt aerosols in the atmosphere: 1. Model development. *J. Geophys. Res.*, **102**, 3819–3830.
- Heintzenberg, J., 1980: Particle size distribution and optical properties of Arctic haze. *Tellus*, **32**, 251–260.
- , and D. Covert, 1987: Chemically resolved submicrometer size distribution and external mixing of the Arctic haze aerosols. *Tellus*, **39B**, 374–382.
- Heymsfield, A., 1972: Ice crystal terminal velocities. *J. Atmos. Sci.*, **29**, 1348–1357.
- Hoff, R. M., W. R. Leitch, P. Fellin, and L. A. Barrie, 1983: Mass size distribution of chemical constituents of the winter Arctic aerosols. *J. Geophys. Res.*, **88**, 10 947–10 956.
- Hudson, J. G., and G. Svensson, 1995: Cloud microphysical relationships in California marine stratus. *J. Appl. Meteor.*, **34**, 2655–2666.
- Khvorostyanov, V. I., and J. A. Curry, 1999: A simple analytical model of aerosol properties with account for hygroscopic growth. Part I: Equilibrium size spectra and CCN activity spectra. *J. Geophys. Res.*, **104**, 2163–2174.
- Lappen, C. L., 1995: Comparison of the CSU GCM modeled climate with observations over the Arctic. Dept. of Atmospheric Sciences Tech Rep., Colorado State University, 200 pp.
- Lax, J. N., and W. Schwerdtfeger, 1976: Terrain-induced vertical motion and occurrence of ice crystal fall at South Pole in summer. *Antarct. J. U.S.*, **9**, 144–145.
- Lohmann, U., N. McFarlane, L. Levkov, K. Abdella, and F. Albers, 1999: Comparing different cloud schemes of a single column model by using mesoscale forcing and nudging technique. *J. Climate*, **12**, 438–461.
- Maxwell, J. B., 1982: Climate of the Canadian Arctic islands and adjacent water. *Climatol. Stud.*, **30**, 34–52.
- McFarlane, N. A., G. J. Boer, J.-P. Blanchet, and M. Lazare, 1992: The Canadian Climate Center second-generation general circulation model and its equilibrium climate. *J. Climate*, **5**, 1013–1044.
- Meyers, M. P., and J. Hallet, 1998: Ice crystal morphology in aircraft contrails and cirrus. Preprints, *14th Conf. on Cloud Physics*, Everett, WA, Amer. Meteor. Soc., 17–20.
- , P. J. DeMott, and W. R. Cotton, 1992: New primary ice-nucleation parameterization in an explicit model. *J. Appl. Meteor.*, **31**, 708–721.
- Novakov, T., C. Rivera-Carpio, J. E. Penner, and C. F. Rogers, 1994: The effect of anthropogenic sulfate aerosols on marine cloud droplet concentrations. *Tellus*, **46B**, 132–141.
- Ohtake, T., and B. E. Holmgren, 1974: Ice crystal from a cloudless sky. Preprints, *Conf. on Cloud Physics*, Tucson, AZ, Amer. Meteor. Soc., 317–320.
- , K. Jayaweera, and K.-I. Sakurai, 1982: Observation of ice crystal formation in lower Arctic atmosphere. *J. Atmos. Sci.*, **39**, 2898–2904.
- Pruppacher, H. R., and J. D. Klett, 1997: *Microphysics of Clouds and Precipitation*. 2d ed. Kluwer Academic Publishers, 955 pp.
- Radke, R. F., C. A. Brock, J. H. Lyons, and P. V. Hobbs, 1989: Aerosol and lidar measurements of hazes in mid-latitude and polar air-masses. *Atmos. Environ.*, **23**, 2417–2430.
- Randall, D. A., K.-M. Xu, R. J. C. Somerville, and S. Iacobellis, 1996: Single column models and cloud ensemble models as links between observations and climate models. *J. Climate*, **9**, 1683–1697.
- Raschke, E., 1987: International Satellite Cloud Climatology Project (ISCCP). WMO Tech. Rep. WMO/TD-170, 131 pp.
- Rogers, R. R., and M. K. Yau, 1989: *A Short Course in Cloud Physics*. 3d ed. Pergamon Press, 293 pp.
- Schnell, R. C., R. G. Barry, M. W. Miles, E. L. Andreas, L. F. Radke, C. A. Brock, M. P. McCormick, and J. L. Moore, 1989: Lidar detection of leads in Arctic sea ice. *Nature*, **339**, 530–532.
- Serzeze, M. C., J. D. Kahl, and R. C. Schnell, 1992: Low-level temperature inversions of the Eurasian Arctic and comparisons with Soviet drifting station data. *J. Climate*, **5**, 615–629.

- Sirois, A., and L. A. Barrie, 1999: Arctic lower tropospheric aerosol trends and composition at Alert, Canada: 1980–1995. *J. Geophys. Res.*, **104**, 3840–3852.
- Trivett, N. B. A., L. A. Barrie, J. W. Bottenheim, J.-P. Blanchet, G. den Hartog, R. M. Hoff, and R. E. Mickle, 1988: An experimental investigation of Arctic haze at Alert, NWT, March 1985. *Atmos.–Ocean*, **26**, 341–376.
- Vong, R. J., and D. S. Covert, 1998: Simultaneous observations of aerosol and cloud droplet size spectra in marine stratocumulus. *J. Atmos. Sci.*, **55**, 2180–2192.
- Walsh, J. E., and R. G. Crane, 1992: A comparison of GCM simulations of arctic climate. *Geophys. Res. Lett.*, **19**, 29–32.
- , A. Lynch, and W. Chapman, 1993: A regional model for studies of atmosphere-ocean-ice interactions in the western Arctic. *Meteor. Atmos. Phys.*, **51**, 179–194.
- Witte, H. J., 1968: Airborne observations of cloud particles and infrared flux density in the Arctic. M.S. thesis, Dept. of Atmospheric Sciences, University of Washington, 101 pp.
- Wyser, K., 1998: The effective radius in ice clouds. *J. Climate*, **11**, 1793–1802.